Energetic BEM-FEM coupling for the numerical solution of the damped wave equation

Energetic BEM-FEM coupling for the numerical solution of the damped wave equation

Alessandra Aimi[a], Mauro Diligenti[a], Chiara Guardasoni[a,*]

[a]*Department of Mathematics and Computer Science*
V.le Parco Area delle Scienze, 53/A
43124 Parma
Italy

Abstract

Time-dependent problems modeled by hyperbolic partial differential equations can be reformulated in terms of boundary integral equations and solved via the boundary element method. In this context, the analysis of damping phenomena that occur in many physics and engineering problems is a novelty. Starting from a recently developed energetic space-time weak formulation for the coupling of boundary integral equations and hyperbolic partial differential equations related to wave propagation problems, we consider here an extension for the damped wave equation in layered media. A coupling algorithm is presented, which allows a flexible use of finite element method and boundary element method as local discretization techniques. Stability and convergence, proved by energy arguments, are crucial in guaranteeing accurate solutions for simulations on large time intervals. Several numerical benchmarks, whose numerical results confirm theoretical ones, are illustrated and discussed.

Keywords: Damped Wave Equation, Energetic Weak Formulation, Boundary Element Method, Finite Element Method

1. Introduction

The study of wave propagation modeled by partial differential equations (PDEs) of hyperbolic type and by systems of boundary integral equations (BIEs) is important in many physics and engineering problems [1, 2, 3, 4, 5, 6].

*Corresponding author. Email address: chiara.guardasoni@unipr.it

The analysis of damping phenomena that occur, for example, in fluid dynamics, in kinetic theory and in semiconductors, is of particular interest: the dissipation is generated by the interaction of the waves with the propagation medium and can be also closely related to the dispersion, as in the interactions between water streams and surface waves or in ferromagnetic materials.
In the context of Boundary Element Method (BEM) the analysis of dissipation through damped wave equation is an almost new topic because it has been scarcely investigated until now. For the numerical solution of the problems that involve this equation, one needs consistent approximations and accurate simulations even on large time intervals. Furthermore, as wave propagation phenomena are often observed in semi-infinite media (domain) where Sommerfeld radiation condition holds, a suitable numerical method has to ensure that this condition is not violated. For example, Finite Element Methods (that are standards in this framework) need the application of special techniques to fulfill this condition that, on the contrary, is implicitly fulfilled by BEM.
In principle, both frequency-domain and time-domain BEM can be used for hyperbolic boundary value problems ([7, 8, 9, 10]). Space-time BEM has the advantage that it directly yields the unknown time-dependent quantities. In this last approach, the construction of the BIEs, via representation formula in terms of single and double layer potentials, uses the fundamental solution of the hyperbolic partial differential equation and jump relations (see e.g. [11, 12, 13, 14, 15, 16]).
For the numerical solution of the damped wave equation in bounded and unbounded layered media, we consider here the extension of the so-called energetic BEM-FEM coupling, recently introduced for the undamped wave equation in one, two e three space dimension ([17, 18, 19]) and for the 1D Klein-Gordon equation in [20]. Coupled BEM-FEM formulations combine the advantages of BEM and FEM methods and eliminate their shortcomings. This approximation technique is based on a weak formulation directly expressed in the space-time domain, thus avoiding the use of the Laplace transform and of its inversion suggested in [14]. The mathematical background of time-dependent boundary integral equations is summarized by M. Costabel in [21].
At the author's knowledge, the consideration of both viscous and material damping terms in the time-domain Galerkin boundary element approach is a novelty. As done for the undamped wave problem [11, 17] and for the Klein-

Gordon equation [20], the analysis is here carried out in one space dimension because it allows to fully understand the approximation technique for what concerns marching on time, avoiding space integration with BEM singular kernels and it is considered as a touchstone for the extension to higher space dimensions.
The paper is structured as follows: at first, we present the model problem on an unbounded 1D layered domain and its energetic weak formulation, then we illustrate the consequent BEM-FEM discretization and we describe the main theoretical results about stability and convergence of the numerical scheme, proved by energy arguments. These properties are crucial in guaranteeing accurate solutions for simulations on large time intervals. The case of a bounded layered domain is then taken into account. At last, a wide variety of significant numerical benchmarks are introduced and discussed.

2. MODEL PROBLEM AND ENERGETIC COUPLING

Let $\Omega = (0, +\infty) \subset \mathbb{R}$ be an open unbounded one dimensional domain, modeling a 3D rod with a dimension, the length along the x-direction, much greater than the remaining ones, with boundary $\Gamma_N := \{x : x = 0\}$. Let $\Omega_1 \cup \Omega_2 = \Omega$ be a decomposition of Ω, with $\Omega_1 = (0, L_1)$ bounded and $\Omega_2 = (L_1, +\infty)$ unbounded non-overlapping subdomains such that $\bar{\Omega}_1 \cap \bar{\Omega}_2 = \Gamma := \{x : x = L_1\}$. Note that the boundary of the unbounded subdomain Ω_2 is just the interface point Γ.
Having denoted by $u_i(x,t)$ the unknown function in the i-th subdomain, which depends on space and time, and with $p_i(x,t) := \dfrac{\partial u_i}{\partial \mathbf{n}_x}(x,t)$, which depends on a unitary outward normal vector $\mathbf{n}_x$ w.r.t. the transversal section of the rod, we want to solve the following wave propagation model problem:

$$\Big(\frac{\partial^2 u_i}{\partial x^2} - \frac{1}{c_i^2}\ddot{u}_i - \frac{2D_i}{c_i^2}\dot{u}_i - \frac{P_i}{c_i^2}u_i\Big)(x,t) = f_i(x,t), \qquad x \in \Omega_i,\ t \in [0,T],\ i = 1,2 \tag{1}$$

$$u_i(x,0) = 0, \qquad x \in \Omega_i,\ i = 1,2 \tag{2}$$

$$\dot{u}_i(x,0) = 0, \qquad x \in \Omega_i,\ i = 1,2 \tag{3}$$

$$p_1(0,t) = \bar{p}(t), \qquad t \in [0,T], \tag{4}$$

where overhead dots indicate derivatives with respect to time, c_i is the propagation velocity of a perturbation in the i-th subdomain, $D_i > 0$ and $P_i > 0$ represent viscous and material damping coefficients, respectively, in Ω_i, $\bar{p}(t)$

is a given function, and, at last, the assigned PDE right-hand sides $f_1(x,t)$ and $f_2(x,t) \equiv 0$ are suitably connected at interface. Moreover, at the interface Γ, the matching conditions read:

$$u_1(L_1,t) = u_2(L_1,t), \qquad c_1^2 p_1(L_1,t) = -c_2^2 p_2(L_1,t), \quad t \in [0,T]. \tag{5}$$

The unknown functions u_i are understood in a weak sense, i.e.

$$u_i \in H^1([0,T]; H^1(\Omega_i)).$$

Since the goal of this work is to approximate u_1 using a FEM approach and u_2 using a BEM technique, we have to obtain a boundary integral reformulation of the problem (1)-(3) in Ω_2.
For this purpose, using classical arguments [21], let us consider the general space-time integral representation formula of $u_2(x,t)$, $x \in \Omega_2$, $t \in [0,T]$:

$$u_2(x,t) = \int_\Gamma \int_0^t G(x,y;t,\tau) p_2(y,\tau) d\tau dy - \int_\Gamma \int_0^t \frac{\partial G}{\partial \mathbf{n}_y}(x,y;t,\tau) u_2(y,\tau) d\tau dy\,, \tag{6}$$

where

$$G(x,y;t,\tau) = \frac{c_2}{2} e^{-D_2(t-\tau)} I_0\left[x,y;t,\tau\right] H[c_2(t-\tau) - |x-y|] \tag{7}$$

is the forward fundamental solution of the damped wave equation (1) on the real line, with $H[\cdot]$ the Heaviside distribution and

$$I_0[x,y;t,\tau] = \sum_{n=0}^{+\infty} \frac{\left[\frac{\sqrt{D_2^2 - P_2}}{c_2} \sqrt{c_2^2(t-\tau)^2 - (x-y)^2}\right]^{2n}}{\left(2^n n!\right)^2} \tag{8}$$

the modified Bessel function of order 0, depending on the subdomain Ω_2 parameters.
Further, let us consider the normal derivative of the representation formula (6), for $x \in \Omega_2$, $t \in [0,T]$:

$$p_2(x,t) = \int_\Gamma \int_0^t \frac{\partial G}{\partial \mathbf{n}_x}(x,y;t,\tau) p_2(y,\tau) d\tau dy - \int_\Gamma \int_0^t \frac{\partial^2 G}{\partial \mathbf{n}_x \partial \mathbf{n}_y}(x,y;t,\tau) u_2(y,\tau) d\tau dy\,. \tag{9}$$

Of course, for the considered model problem, integrals over Γ in (6) and in (9) collapse into simple collocations in $y = L_1$.
Derivatives in (6), (9) have to be understood in a distributional sense. In particular, by means of relations

$$\frac{\partial I_0[x,y;t,\tau]}{\partial x} = -\frac{\partial I_0[x,y;t,\tau]}{\partial y} = \frac{\partial I_0[x,y;t,\tau]}{\partial \tau} \frac{x-y}{c_2^2(t-\tau)}\,, \tag{10}$$

$$\begin{aligned}\frac{\partial H[c_2(t-\tau)-|x-y|]}{\partial x} &= -\frac{\partial H[c_2(t-\tau)-|x-y|]}{\partial y} \\ &= \frac{\partial H[c_2(t-\tau)-|x-y|]}{\partial \tau}\frac{x-y}{c_2|x-y|}\,, \end{aligned} \tag{11}$$

we obtain

$$\begin{aligned}\frac{\partial G}{\partial \mathbf{n}_y}(x,y;t,\tau) &= \frac{\mathbf{n}_y}{2}e^{-D_2(t-\tau)}\Big\{c_2\frac{x-y}{|x-y|}\delta[c_2(t-\tau)-|x-y|]I_0[x,y;t,\tau] \\ &+ (x-y)\frac{\sqrt{D_2^2-P_2}\; I_1[x,y;t,\tau]}{\sqrt{c_2^2(t-\tau)^2-(x-y)^2}}H[c_2(t-\tau)-|x-y|]\Big\}, \end{aligned} \tag{12}$$

with

$$I_1[x,y;t,\tau]=\sum_{n=0}^{+\infty}\frac{\left[\frac{\sqrt{D_2^2-P_2}}{c_2}\sqrt{c_2^2(t-\tau)^2-(x-y)^2}\right]^{2n+1}}{2(n+1)(2^n n!)^2}$$

the modified Bessel functions of order 1, depending on the subdomain Ω_2 parameters; analogously,

$$\begin{aligned}\frac{\partial G}{\partial \mathbf{n}_x}(x,y;t,\tau) &= -\frac{\mathbf{n}_x}{2}e^{-D_2(t-\tau)}\Big\{c_2\frac{x-y}{|x-y|}\delta[c_2(t-\tau)-|x-y|]I_0[x,y;t,\tau] \\ &+ (x-y)\frac{\sqrt{D_2^2-P_2}\; I_1[x,y;t,\tau]}{\sqrt{c_2^2(t-\tau)^2-(x-y)^2}}H[c_2(t-\tau)-|x-y|]\Big\}, \end{aligned} \tag{13}$$

and finally

$$\begin{aligned}\frac{\partial^2 G}{\partial \mathbf{n}_x\partial \mathbf{n}_y}(x,y;t,\tau) &= \frac{\mathbf{n}_x\mathbf{n}_y}{2}e^{-D_2(t-\tau)}\Big\{\frac{\sqrt{D_2^2-P_2}\; I_1[x,y;t,\tau]}{\sqrt{c_2^2(t-\tau)^2-(x-y)^2}}H[c_2(t-\tau)-|x-y|] \\ &- (x-y)^2\frac{D_2^2-P_2}{c_2}\frac{I_1'[x,y;t,\tau]}{c_2^2(t-\tau)^2-(x-y)^2}H[c_2(t-\tau)-|x-y|] \\ &+ (x-y)^2\frac{\sqrt{D_2^2-P_2}\; I_1[x,y;t,\tau]}{\sqrt{(c_2^2(t-\tau)^2-(x-y)^2)^3}}H[c_2(t-\tau)-|x-y|] \\ &- 2|x-y|\frac{\sqrt{D_2^2-P_2}\; I_1[x,y;t,\tau]}{\sqrt{c_2^2(t-\tau)^2-(x-y)^2}}\delta[c_2(t-\tau)-|x-y|] \\ &+ \frac{\partial}{\partial\tau}\delta[c_2(t-\tau)-|x-y|]I_0[x,y;t,\tau]\Big\}\,. \end{aligned} \tag{14}$$

In (14)

$$I_1'[x,y;t,\tau]=\frac{I_1[x,y;t,\tau]}{\frac{\sqrt{D_2^2-P_2}}{c_2}\sqrt{c_2^2(t-\tau)^2-(x-y)^2}}+I_2[x,y;t,\tau]\,,$$

where $I_2[x,y;t,\tau] := I_2\Big(\frac{\sqrt{D_2^2-P_2}}{c_2}\sqrt{c_2^2(t-\tau)^2-(x-y)^2}\Big)$, being $I_2(\cdot)$ is the modified Bessel function of order 2.
Now, we can substitute (7), (12), (13) and (14) into (6) and (9), respectively, to write the explicit expressions of the representation formulas for $u_2(x,t)$ and $p_2(x,t)$. For instance, for what concerns (6), one gets

$$\begin{aligned} u_2(x,t) &= \int_0^{t-\frac{x-L_1}{c_2}} \frac{c_2}{2} e^{-D_2(t-\tau)} I_0[x,L_1;t,\tau] p_2(L_1,\tau) d\tau \\ &- \mathbf{n}_y \int_0^{t-\frac{x-L_1}{2}} \frac{x-L_1}{c_2} e^{-D_2(t-\tau)} \frac{\sqrt{D_2^2-P_2}\, I_1[x,L_1;t,\tau]}{\sqrt{c_2^2(t-\tau)^2-(x-L_1)^2}} u_2(L_1,\tau) d\tau \\ &- \frac{\mathbf{n}_y}{2} u_2(L_1, t-\frac{x-L_1}{c_2}) e^{-D_2\frac{x-L_1}{c_2}} . \end{aligned} \tag{15}$$

Analogously, one can rewrite (9) and, at this stage, taking the limit as $x \to L_1^+$, after some simple analytic computations, problem (1)-(3) in the subdomain Ω_2 can be rewritten as a system of two BIEs in the boundary unknowns the functions $p_2(L_1,t)$ and $u_2(L_1,t)$:

$$\begin{cases} u_2(L_1,t) = (\mathcal{V}p_2)(L_1,t) \\ p_2(L_1,t) = (\mathcal{D}u_2)(L_1,t) \end{cases} \qquad t \in [0,T]\,, \tag{16}$$

where

$$\begin{aligned} (\mathcal{V}p_2)(L_1,t) &= c_2 \int_0^t e^{-D_2(t-\tau)} I_0[L_1,L_1;t,\tau] p_2(L_1,\tau) d\tau\,, \\ (\mathcal{D}u_2)(L_1,t) &= \frac{D_2}{c_2}\, u_2(L_1,t) + \frac{1}{c_2}\dot{u}_2(L_1,t) \\ &- \frac{\sqrt{D_2^2-P_2}}{c_2} \int_0^t e^{-D_2(t-\tau)} \frac{I_1[L_1,L_1;t,\tau]}{t-\tau}\, u_2(L_1,\tau) d\tau\,. \end{aligned} \tag{17}$$

Of course, problem (16) has to be coupled with the differential one specified in Ω_1, under the coupling conditions (5) at the interface. In particular, here we are interested in a direct space-time energetic weak formulation for the coupling of the integro-differential problem on $\Omega_1 \cup \Omega_2$, and this will be done in the following, extending what has been done in [19, 20].
We observe that the solution of the damped wave equation in Ω_2 satisfies the

following energy identity:

$$\mathcal{E}_{\Omega_2}(u_2,T) := \frac{1}{2}\int_{\Omega_2}\left[\left(\frac{\partial u_2(x,T)}{\partial x}\right)^2 + \frac{1}{c_2^2}\dot{u}_2^2(x,T) + \frac{P_2}{c_2^2}u_2^2(x,T) + \frac{4D_2}{c_2^2}\int_0^T \dot{u}_2^2(x,t)dt\right]dx$$
$$= \int_0^T \dot{u}_2(L_1,t)p_2(L_1,t)\,dt \geq 0\,, \tag{18}$$

which can be obtained multiplying equation (1) by $\dot{u}_2$ and integrating by parts over $\Omega_2 \times [0,T]$.
Then, taking into account the last term in (18) and the nature of the two equations in the system (16), their energetic weak formulation is:

find $u_2(L_1,t) \in H^1([0,T])$ *and* $p_2(L_1,t) \in L^2([0,T])$ *such that*

$$\begin{cases} \langle \dot{u}_2, q_2\rangle = \langle (\dot{\mathcal{V}p_2}), q_2\rangle \\ \langle p_2, \dot{v}_2\rangle = \langle \mathcal{D}u_2, \dot{v}_2\rangle, \end{cases} \tag{19}$$

where $\langle\cdot,\cdot\rangle := \langle\cdot,\cdot\rangle_{L^2([0,T])}$ and $q_2(L_1,t)$, $v_2(L_1,t)$ are test functions belonging to the same functional space of $p_2(L_1,t)$ and $u_2(L_1,t)$, respectively. In particular, the first equation in (16) has been differentiated with respect to time and projected with the $L^2([0,T])$ scalar product by means of functions belonging to $L^2([0,T])$, while the second equation in (16) has been projected with the $L^2([0,T])$ scalar product by means of functions belonging to $H^1([0,T])$, derived with respect to time.
For the energetic weak formulation in Ω_1, let us multiply the differential equation (1) for the time derivative of test function $v_1(x,t) \in H^1([0,T]; H^1(\Omega_1))$ and integrate by parts in space obtaining:

$$-\mathcal{A}(u_1,v_1) + \langle \dot{v}_{1|_\Gamma},\, p_{1|_\Gamma}\rangle = \mathcal{F}(v_1) - \langle \dot{v}_{1|_{\Gamma_N}},\, \bar{p}\rangle, \tag{20}$$

where

$$\mathcal{A}(u_1,v_1) := \int_0^T\int_{\Omega_1}\Big(\frac{\partial \dot{v}_1}{\partial x}\,\frac{\partial u_1}{\partial x} + \frac{1}{c_1^2}\dot{v}_1\ddot{u}_1 + \frac{2D_1}{c_1^2}\dot{v}_1\dot{u}_1 + \frac{P_1}{c_1^2}\dot{v}_1 u_1\Big)(x,t)\,dx\,dt\,, \tag{21}$$

$$\mathcal{F}(v_1) := \int_0^T\int_{\Omega_1}\dot{v}_1(x,t)f_1(x,t)\,dx\,dt\,. \tag{22}$$

Now, remembering the interface condition (5), using the further coupling condition at interface $v_1(L_1,t) = v_2(L_1,t)$ for test functions and combining (20) with the second weak BIE in (19), multiplied by c_2^2, we finally obtain

the following energetic weak formulation of the coupled problem:

$$\begin{cases} \langle (\dot{\mathcal{V}} p_2), q_2 \rangle - \langle \dot{u}_{1|\Gamma}, q_2 \rangle = 0 \\ -\langle p_2, \dot{v}_{1|\Gamma} \rangle - \langle \mathcal{D} u_{1|\Gamma}, \dot{v}_{1|\Gamma} \rangle - 2\frac{c_1^2}{c_2^2}\mathcal{A}(u_1, v_1) = 2\frac{c_1^2}{c_2^2}\mathcal{F}(v_1) - 2\frac{c_1^2}{c_2^2}\langle \dot{v}_{1|\Gamma_N}, \bar{p} \rangle \,. \end{cases} \tag{23}$$

At every time instant, the unknowns are u_1 in $\overline{\Omega}_1$ and p_2 at the interface point $x = L_1$.
Let us conclude this Section with some energy considerations. At first, let us consider system (19) with $q_2 = p_2$ and $v_2 = u_2$; then, summing up the two equation and remembering (18) one obtains:

$$\langle \dot{u}_2, p_2 \rangle = \frac{1}{2}(\langle (\dot{\mathcal{V}} p_2), p_2 \rangle + \langle \mathcal{D} u_2, u_2 \rangle) = \mathcal{E}_{\Omega_2}(u_2, T). \tag{24}$$

On the other side, considering $v_1 = u_1$ in (21), one gets:

$$\mathcal{A}(u_1, u_1) = \mathcal{E}_{\Omega_1}(u_1, T), \tag{25}$$

where $\mathcal{E}_{\Omega_1}(u_1, T)$ is defined as in (18).
Following similar arguments, starting from (23) the following relation appears:

$$c_1^2 \mathcal{E}_{\Omega_1}(u_1, T) + c_2^2 \mathcal{E}_{\Omega_2}(u_2, T) = -c_1^2 \mathcal{F}(u_1) + c_1^2 \langle \dot{u}_{1|\Gamma_N}, \bar{p} \rangle, \tag{26}$$

from which one can deduce a-priori stability estimates for regular solutions u_1 and u_2 bounding from above the related energies by means of the problem data (the interest reader is referred to [20] for mathematical details of this analysis).

3. SPACE-TIME GALERKIN APPROXIMATION

For time discretization we consider a uniform decomposition of the time interval $[0, T]$ with time step $\Delta t = T/N_{\Delta t}$, $N_{\Delta t} \in \mathbb{N}^+$, generated by the $N_{\Delta t} + 1$ time instants: $t_k = k\Delta t$, $k = 0, \ldots, N_{\Delta t}$ and we choose piecewise constant shape functions for the time approximation of p_2 and piecewise linear shape functions for the time approximation of u_1, although higher degree shape functions can be used. In particular, for $k = 0, \ldots, N_{\Delta t} - 1$, time shape functions for the approximation of p_2 and u_1 will be defined respectively as:

$$\bar{\psi}_k(t) = H[t - t_k] - H[t - t_{k+1}]\,, \qquad \hat{\psi}_k(t) = R(t - t_k) - R(t - t_{k+1}), \tag{27}$$

where $R(t-t_k) = \dfrac{t-t_k}{\Delta t} H[t-t_k]$ is the ramp function.
For the space discretization we consider the bounded subdomain Ω_1 suitably decomposed by means of a mesh $\mathcal{T}_{\Delta x} = \{e_1, \ldots, e_{N_{\Delta x}}\}$ constituted by $N_{\Delta x}$ straight elements, with $length(e_i) \leq \Delta x$, $e_i \cap e_j = \emptyset$ if $i \neq j$ and such that $\cup_{i=1}^{N_{\Delta x}} \bar{e}_i = \bar{\Omega}_1$.
The functional background compels one to choose spatial shape functions belonging to $C^0(\Omega_1)$ for the approximation of u_1. Hence, we will choose piecewise linear continuous functions $\hat{\varphi}_j(x)$, $j = 0, \ldots, N_{\Delta x}$ related to $\mathcal{T}_{\Delta x}$ for the approximation of u_1 in Ω_1.
The approximate solutions of the problem at hand, for $t \in [0, T]$, will be expressed as:

$$\begin{aligned} p_2(L_1, t) &\approx \tilde{p}_2(L_1, t) = \sum_{k=0}^{N_{\Delta t}-1} \alpha_k \bar{\psi}_k(t), \\ u_1(x, t) &\approx \tilde{u}_1(x, t) = \sum_{k=0}^{N_{\Delta t}-1} \hat{\psi}_k(t) \sum_{j=0}^{N_{\Delta x}} \beta_{kj} \hat{\varphi}_j(x) =: \sum_{k=0}^{N_{\Delta t}-1} \hat{\psi}_k(t) \hat{\Phi}_k(x), \quad x \in \Omega_1. \end{aligned} \tag{28}$$

The discretization of the energetic weak formulation (23) produces the linear system $\mathrm{M}\,\mathrm{x} = \mathrm{y}$, where matrix M has a block lower triangular Toeplitz structure since its elements depend on the difference $t_h - t_k$ and in particular they vanish if $t_h < t_k$, as frequently pointed out for the energetic BEM-FEM applied to undamped wave propagation problems (see [17, 18, 19]):

$$\begin{pmatrix} \mathrm{M}^{(0)} & 0 & 0 & \cdots & 0 \\ \mathrm{M}^{(1)} & \mathrm{M}^{(0)} & 0 & \ldots & 0 \\ \mathrm{M}^{(2)} & \mathrm{M}^{(1)} & \mathrm{M}^{(0)} & \ldots & 0 \\ \ldots & \ldots & \ldots & \ddots & \vdots \\ \mathrm{M}^{(N_{\Delta t}-1)} & \mathrm{M}^{(N_{\Delta t}-2)} & \mathrm{M}^{(N_{\Delta t}-3)} & \ldots & \mathrm{M}^{(0)} \end{pmatrix} \begin{pmatrix} \mathrm{x}^{(0)} \\ \mathrm{x}^{(1)} \\ \mathrm{x}^{(2)} \\ \vdots \\ \mathrm{x}^{(N_{\Delta t}-1)} \end{pmatrix} = \begin{pmatrix} \mathrm{y}^{(0)} \\ \mathrm{y}^{(1)} \\ \mathrm{y}^{(2)} \\ \vdots \\ \mathrm{y}^{(N_{\Delta t}-1)} \end{pmatrix} \tag{29}$$

and the unknowns are organized as follows:

$$\mathrm{x}^{(\ell)} = \left(\alpha_\ell,\, \beta_{\ell 0},\, \beta_{\ell 1}, \ldots, \beta_{\ell N_{\Delta x}}\right)^\top, \qquad \ell = 0, \ldots, N_{\Delta t} - 1\,.$$

Note that, with this choice of basis, each block is symmetric and it has the following structure:

$$\mathrm{M}^{(\ell)} = \begin{pmatrix} \mathrm{M}_\Gamma^{(\ell)} & \mathrm{M}_{\Gamma,FEM}^{(\ell)} \\ \mathrm{M}_{FEM,\Gamma}^{(\ell)} & \mathrm{M}_{FEM}^{(\ell)} \end{pmatrix}$$

where diagonal sub-blocks have dimensions 2, $N_{\Delta x}$, respectively, and whose elements have been evaluated numerically by means of adaptive Simpson rule.
In [20], it has been proved by energy arguments, that the numerical scheme coming from energetic BEM-FEM coupling, applied to the simpler one-dimensional Klein-Gordon equation (i.e. the PDE in (1) without the term involving the first order time derivative of the unknown), is unconditionally stable and convergent, under suitable regularity assumptions for the problem data. In particular, it holds:

$$\begin{aligned} E_{\Delta t,\Delta x} &:= \max_k \|\tilde{u}_1(\cdot,t_k) - u_1(\cdot,t_k)\|_{H^1(\Omega_1)} + \|\tilde{p}_2(L_1,\cdot) - p_2(L_1,\cdot)\|_{L^2([0,T])} \\ &= O(\Delta x) + O(\Delta t)\,. \end{aligned} \tag{30}$$

This error estimate holds for the complete damping equation (1) too, since with the position $u_i(x,t) = e^{-D_i t} w_i(x,t)$, equation (1) can be formally reduced to the Klein-Gordon equation in the unknown function $w_i(x,t)$.
In the following Section, we derive, using simple mathematical tools, a stability result for the presented numerical method directly applied to the damped problem.

4. Energy estimates for the numerical scheme

Let us consider the second energetic weak equation in (23), which involves all the problem unknowns, and, to simplify the following notation, $\bar{p} = 0$. Now, using (28) as approximate solutions and $v_1(x,t) = \hat{\psi}_h(t)\hat{\Phi}_h(x)$ as test function ($h = 0, \ldots, N_{\Delta t} - 1$), remembering the second weak BIE in (19), after a straightforward substitution, we obtain

$$\begin{aligned} &\hat{\Phi}_h(L_1) \sum_{k=0}^{N_{\Delta t}-1} \alpha_k \int_0^T \dot{\hat{\psi}}_h(t)\bar{\psi}_k(t)\,dt + \frac{c_1^2}{c_2^2} \sum_{k=0}^{N_{\Delta t}-1} \Big[\langle \hat{\Phi}_h', \hat{\Phi}_k' \rangle_{L^2(\Omega_1)} \int_0^T \dot{\hat{\psi}}_h(t)\hat{\psi}_k(t)\,dt \\ &+ \frac{\langle \hat{\Phi}_h, \hat{\Phi}_k \rangle_{L^2(\Omega_1)}}{c_1^2} \int_0^T \{\dot{\hat{\psi}}_h(t)\ddot{\hat{\psi}}_k(t) + 2D_1\,\dot{\hat{\psi}}_h(t)\dot{\hat{\psi}}_k(t) + P_1\,\dot{\hat{\psi}}_h(t)\hat{\psi}_k(t)\}\,dt \Big] \\ &= \frac{c_1^2}{c_2^2}\,(\hat{\Phi}_h, F_h)_{L^2(\Omega_1)}\,, \end{aligned} \tag{31}$$

where $F_h(x) = -\displaystyle\int_0^T \dot{\hat{\psi}}_h(t)\, f_1(x,t)\,dt$ and the inverted commas represent derivatives with respect to variable x.

Performing analytically time integrals in the left-hand side of (31), we get:

$$c_2^2\hat{\Phi}_h(L_1)\alpha_h + c_1^2\sum_{k=0}^{h-1}\langle\hat{\Phi}'_h,\hat{\Phi}'_k\rangle_{L^2(\Omega_1)} + \frac{c_1^2}{2}\,\langle\hat{\Phi}'_h,\hat{\Phi}'_h\rangle_{L^2(\Omega_1)} + \langle\hat{\Phi}_h,\frac{\hat{\Phi}_h-\hat{\Phi}_{h-1}}{\Delta\,t^2}\rangle_{L^2(\Omega_1)}$$
$$+2D_1\,\frac{\langle\hat{\Phi}_h,\hat{\Phi}_h\rangle_{L^2(\Omega_1)}}{\Delta\,t} + P_1\sum_{k=0}^{h-1}\langle\hat{\Phi}_h,\hat{\Phi}_k\rangle_{L^2(\Omega_1)} + \frac{P_1}{2}\,\langle\hat{\Phi}_h,\hat{\Phi}_h\rangle_{L^2(\Omega_1)}$$
$$= c_1^2\,\langle\hat{\Phi}_h,F_h\rangle_{L^2(\Omega_1)}\,. \tag{32}$$

At this stage we need to observe that, from (28),

$$p_{2,h} := \tilde{p}_2(L_1,t_h) = \alpha_h, \quad u_{1,h}(x) := \widetilde{u}_1(x,t_h) = \sum_{k=0}^{h-1}\hat{\Phi}_k(x) \tag{33}$$

and

$$u_{1,h+1}(x) - u_{1,h}(x) = \hat{\Phi}_h(x)\,; \tag{34}$$

hence we can rewrite the numerical scheme (32) as

$$c_2^2(u_{1,h+1}(L_1)-u_{1,h}(L_1))p_{2,h} + c_1^2\,\langle u'_{1,h+1}-u'_{1,h},\frac{u'_{1,h+1}+u'_{1,h}}{2}\rangle_{L^2(\Omega_1)}$$
$$+\langle u_{1,h+1}-u_{1,h},\frac{u_{1,h+1}-2u_{1,h}+u_{1,h-1}}{\Delta\,t^2}\rangle_{L^2(\Omega_1)}$$
$$+2D_1\,\langle u_{1,h+1}-u_{1,h},\frac{u_{1,h+1}-u_{1,h}}{\Delta\,t}\rangle_{L^2(\Omega_1)} + P_1\,\langle u_{1,h+1}-u_{1,h},\frac{u_{1,h+1}+u_{1,h}}{2}\rangle_{L^2(\Omega_1)}$$
$$= c_1^2\,\langle u_{1,h+1}-u_{1,h},F_h\rangle_{L^2(\Omega_1)}\,. \tag{35}$$

Remark. Here, we want to stress the fact that the proposed energetic weak formulation, after time integration, can be regarded as a Newmark scheme for the differential part of the coupling. In fact, starting from the second term in the left-hand side of (35) we can recognize a semi-discretization in time for the problem in the subdomain Ω_1, operated through the cited technique with parameters $\zeta = \frac{1}{2}$, $\theta = 1$ in the notation of [22]. This particular Newmark scheme is implicit, unconditionally stable and first order accurate in $\Delta\,t$.

Now, having set $\|\cdot\| = \|\cdot\|_{L^2(\Omega_i)}$, let us introduce the discrete energy in the subdomain Ω_i, $i = 1,2$, at the time instant t_h, defined as

$$\mathcal{E}^h_{\Omega_i} := \frac{1}{2c_i^2}\left[\|\frac{u_{i,h}-u_{i,h-1}}{\Delta\,t}\|^2 + c_i^2\|u'_{i,h}\|^2 + P_i\,\|u_{i,h}\|^2 + 4D_i\,\Delta\,t\sum_{k=0}^{h}\|\frac{u_{i,k}-u_{i,k-1}}{\Delta\,t}\|^2\right], \tag{36}$$

which really represents a discretization of the definition (18), given above for the subdomain Ω_2. Further we observe that:

$$\langle u_{1,h+1} - u_{1,h}, u_{1,h+1} + u_{1,h} \rangle_{L^2(\Omega_1)} = \|u_{1,h+1}\|^2 - \|u_{1,h}\|^2$$

and analogously for the related space derivatives, i.e.

$$\langle u'_{1,h+1} - u'_{1,h}, u'_{1,h+1} + u'_{1,h} \rangle_{L^2(\Omega_1)} = \|u'_{1,h+1}\|^2 - \|u'_{1,h}\|^2 ;$$

moreover

$$\begin{aligned}
&\langle u_{1,h+1} - u_{1,h}, u_{1,h+1} - 2u_{1,h} + u_{1,h-1} \rangle_{L^2(\Omega_1)} \\
&\quad = \|u_{1,h+1} - u_{1,h}\|^2 - \langle u_{1,h+1} - u_{1,h},\, u_{1,h} - u_{1,h-1} \rangle_{L^2(\Omega_1)} \\
&\quad \geq \|u_{1,h+1} - u_{1,h}\|^2 - \frac{1}{2}\|u_{1,h+1} - u_{1,h}\|^2 - \frac{1}{2}\|u_{1,h} - u_{1,h-1}\|^2 \\
&\quad = \frac{1}{2}\|u_{1,h+1} - u_{1,h}\|^2 - \frac{1}{2}\|u_{1,h} - u_{1,h-1}\|^2 .
\end{aligned}$$

Combining these results with (35) and (36), we obtain:

$$c_2^2 (u_{1,h+1}(L_1) - u_{1,h}(L_1)) p_{2,h} + c_1^2 [\mathcal{E}^{h+1}_{\Omega_1} - \mathcal{E}^{h}_{\Omega_1}] \leq c_1^2 \langle u_{1,h+1} - u_{1,h}, F_h \rangle_{L^2(\Omega_1)} . \quad (37)$$

Now, applying Cauchy-Schwarz inequality to the right-hand side of (37) we get

$$c_2^2 (u_{1,h+1}(L_1) - u_{1,h}(L_1)) p_{2,h} + c_1^2 [\mathcal{E}^{h+1}_{\Omega_1} - \mathcal{E}^{h}_{\Omega_1}] \leq c_1^2 \, \Delta t \, \sqrt{2} \, \| \frac{u_{1,h+1} - u_{1,h}}{\sqrt{2}\, c_1 \Delta t} \| \, \| c_1 \, F_h \| , \quad (38)$$

from which, remembering (36), we deduce

$$c_2^2 (u_{1,h+1}(L_1) - u_{1,h}(L_1)) p_{2,h} + c_1^2 [\mathcal{E}^{h+1}_{\Omega_1} - \mathcal{E}^{h}_{\Omega_1}] \leq c_1^2 \, \Delta t \, \mathcal{E}^{h+1}_{\Omega_1} + c_1^4 \, \frac{\Delta t}{2} \|F_h\|^2 . \quad (39)$$

Let us now sum inequality (39), for $h = 0, \cdots, n-1$, with $n \leq N_{\Delta t}$, observing that $\mathcal{E}^0_{\Omega_1} = 0$:

$$\begin{aligned}
&c_2^2 \, \Delta t \sum_{h=0}^{n-1} \frac{u_{1,h+1}(L_1) - u_{1,h}(L_1)}{\Delta t} \, p_{2,h} + c_1^2 \, \mathcal{E}^n_{\Omega_1} \\
&\quad \leq \; c_1^2 \, \Delta t \, \mathcal{E}^n_{\Omega_1} + c_1^2 \Delta t \sum_{h=0}^{n-1} \mathcal{E}^h_{\Omega_1} + c_1^4 \, \frac{\Delta t}{2} \sum_{h=0}^{n-1} \|F_h\|^2 . \qquad (40)
\end{aligned}$$

Let us note that, remembering the coupling conditions (5) on the interface $x = L_1$ and (18), for the first term in the left-hand side of (40) it holds, for sufficiently small $\Delta\, t$,

$$\Delta\, t \sum_{h=0}^{n-1} \frac{u_{2,h+1}(L_1) - u_{2,h}(L_1)}{\Delta\, t}\, p_{2,h} \simeq \int_0^{t_n} \dot{u}_2(L_1, t) p_2(L_1, t)\, dt = \mathcal{E}_{\Omega_2}(u_2, t_n)\,, \quad (41)$$

hence we can write

$$\Delta\, t \sum_{h=0}^{n-1} \frac{u_{2,h+1}(L_1) - u_{2,h}(L_1)}{\Delta\, t}\, p_{2,h} = \mathcal{E}^n_{\Omega_2} \geq 0 \quad (42)$$

and finally from (40) and (42)

$$c_1^2\,(1 - \Delta\, t)\, \mathcal{E}^n_{\Omega_1} + c_2^2\, \mathcal{E}^n_{\Omega_2} \leq c_1^2\, \Delta\, t \sum_{h=0}^{n-1} \mathcal{E}^h_{\Omega_2} + c_1^4\, \frac{\Delta\, t}{2} \sum_{h=0}^{n-1} \|F_h\|^2\,. \quad (43)$$

For the discrete energy in the subdomain Ω_{Ω_1} we obtain, under the natural assumption $\Delta\, t < 1$,

$$\mathcal{E}^n_{\Omega_1} \leq \frac{\Delta\, t}{1 - \Delta\, t} \sum_{h=0}^{n-1} \mathcal{E}^h_{\Omega_1} + \frac{c_1^2\, \Delta\, t}{2(1 - \Delta\, t)} \sum_{h=0}^{n-1} \|F_h\|^2 \quad (44)$$

and, applying at last the discrete Gronwall's Lemma [22], we deduce, for every time instant t_n, the following upper bound:

$$\mathcal{E}^n_{\Omega_1} \leq \frac{c_1^2\, \Delta\, t}{2(1 - \Delta\, t)} \sum_{h=0}^{n-1} \|F_h\|^2\, \exp\Big(\frac{t_n}{1 - \Delta\, t}\Big)\,. \quad (45)$$

If we finally consider the discrete energy in the subdomain Ω_2, from (43) we can write

$$\mathcal{E}^n_{\Omega_2} \leq \frac{c_1^2}{c_2^2}\, \Delta\, t \Big[\sum_{h=0}^{n-1} \mathcal{E}^h_{\Omega_1} + \frac{c_1^2}{2} \sum_{h=0}^{n-1} \|F_h\|^2 \Big] \quad (46)$$

and using (45) to bound from above every term in the first sum on the right-hand side of (46), i.e.

$$\mathcal{E}^n_{\Omega_2} \leq \frac{c_1^4}{2\, c_2^2}\, \Delta\, t \Big\{ \sum_{h=0}^{n-1} \Big[\frac{\Delta\, t}{(1 - \Delta\, t)} \sum_{\ell=0}^{h-1} \|F_\ell\|^2\, \exp\Big(\frac{t_h}{1 - \Delta\, t}\Big) \Big] + \sum_{h=0}^{n-1} \|F_h\|^2 \Big\}\,, \quad (47)$$

we succeed in proving a complete stability result for our numerical scheme, depending on problem data.

5. The case of a bounded bi-domain

Let us consider now the problem (1)-(5) for the one-dimensional linear damped wave equation defined on a bi-material rod $\Omega = (0, L)$ of finite length, decomposed in two bounded subdomains $\Omega_1 = (0, L_1)$ and $\Omega_2 = (L_1, L)$.
In this case the domain Ω_2 is bounded by $\Gamma_2 := \{x : x = L_1, x = L\}$, the interface between Ω_1 and Ω_2 is still $\Gamma := \{x : x = L_1\}$ and we suppose to consider on the right end-point of the rod a Dirichlet condition:

$$u_2(L,t) = \overline{u}(t)\,, \qquad t \in [0,T]. \tag{48}$$

The energetic weak formulation is obtained as for the unbounded rod, considering the differential problem in Ω_1 and an equivalent integral problem in Ω_2. In particular, for this latter, starting from (6) and (9) written on the interface Γ, where both $u_2(L_1,t)$ and $p_2(L_1,t)$ are unknowns, and from (6) written in $x = L$, where $p_2^L(t) := p_2(L,t)$ is unknown too, applying the same energy considerations as before and with some straightforward analytic computations, we obtain the following system of weak equations:

$$\left\langle \begin{bmatrix} \dot{\mathcal{V}} & \dot{\overline{\mathcal{V}}} & -\dot{\mathcal{K}} \\ \dot{\overline{\mathcal{V}}} & \dot{\mathcal{V}} & -\dot{\mathcal{I}} \\ -\mathcal{K} & \mathcal{I} & -\mathcal{D} \end{bmatrix} \begin{bmatrix} p_2^L \\ p_2 \\ u_2 \end{bmatrix}, \begin{pmatrix} q_2^L \\ q_2 \\ \dot{v_2} \end{pmatrix} \right\rangle_{L^2[0,T]} = \left\langle \begin{bmatrix} \dot{\overline{u}} \\ \dot{\mathcal{K}}\overline{u} \\ \overline{\mathcal{D}}\overline{u} \end{bmatrix}, \begin{pmatrix} q_2^L \\ q_2 \\ \dot{v_2} \end{pmatrix} \right\rangle_{L^2[0,T]} \tag{49}$$

where $\mathcal{I}$ is the identity function, $\mathcal{V}$ and $\mathcal{D}$ have been defined in (17),

$$\begin{aligned} (\overline{\mathcal{V}}w)(t) &= c_2 \int_0^{t-L_2/c_2} e^{-D_2(t-\tau)} I_0\left[L, L_1; t, \tau\right] w(\tau) d\tau\,, \\ (\mathcal{K}w)(t) &= -\frac{L_2}{c_2} \int_0^{t-L_2/c_2} I_0\left[L, L_1; t, \tau\right] \frac{\partial}{\partial \tau}\left[e^{-D_2(t-\tau)} \frac{w(\tau)}{t-\tau}\right] d\tau \end{aligned} \tag{50}$$

and

$$\begin{aligned} (\overline{\mathcal{D}}w)(t) = -\frac{1}{c_2} \int_0^{t-L_2/c_2} I_0\left[L_1, L; t, \tau\right] \Bigg\{ \frac{\partial}{\partial \tau}\left[e^{-D_2(t-\tau)} w(\tau)\left(\frac{1}{t-\tau} + \frac{L_2^2}{c_2^2}\frac{1}{(t-\tau)^3}\right)\right] \\ - \frac{L_2^2}{c_2^2}\frac{\partial^2}{\partial \tau^2}\left(e^{-D_2(t-\tau)}\frac{w(\tau)}{(t-\tau)^2}\right)\Bigg\} d\tau\,, \end{aligned} \tag{51}$$

with $L_2 = L - L_1$.
Performing a suitable linear combination between the weak equation (20) related to Ω_1 and the third weak integral equation in (49) and applying coupling conditions (5), the final energetic weak formulation for the coupled

problem, after suitable integrations by parts in time, is the following:

given $\overline{p}(t) \in L^2[0,T]$, $\overline{u}(t) \in H^1[0,T]$,
find $p_2^L(t)$, $p_2(t) \in L^2[0,T]$ *and* $u_1(x,t) \in H^1([0,T], H^1(\Omega_1))$ *such that*
$\forall q_2^L(t), q_2(t) \in L^2[0,T]$ *and* $\forall v_1(x,t) \in H^1([0,T], H^1(\Omega_1))$

$$\begin{cases} \langle \mathcal{A}_{11}[p_2^L], q_2^L \rangle_{L^2[0,T]} + \langle \mathcal{A}_{12}[p_2], q_2^L \rangle_{L^2[0,T]} + \langle \mathcal{A}_{13}[\dot{u}_{1|\Gamma}], q_2^L \rangle_{L^2[0,T]} = \mathcal{F}_1(q_2^L) \\ \\ \langle \mathcal{A}_{21}[p_2^L], q_2 \rangle_{L^2[0,T]} + \langle \mathcal{A}_{22}[p_2], q_2 \rangle_{L^2[0,T]} + \langle \mathcal{A}_{23}[\dot{u}_{1|\Gamma}], q_2 \rangle_{L^2[0,T]} = \mathcal{F}_2(q_2) \\ \\ \langle \mathcal{A}_{31}[p_2^L], \dot{v}_{1|\Gamma} \rangle_{L^2[0,T]} + \langle \mathcal{A}_{32}[p_2], \dot{v}_{1|\Gamma} \rangle_{L^2[0,T]} + \\ \qquad + \langle \mathcal{A}_{33}[\dot{u}_{1|\Gamma}], \dot{v}_{1|\Gamma} \rangle_{L^2[0,T]} - 2\mathcal{A}(u_1, v_1) = \mathcal{F}_3(\dot{v}_1) \end{cases} \tag{52}$$

where:

$$\mathcal{A}_{11}[p_2^L](t) = c_2 \int_0^t e^{-D_2(t-\tau)} I_0 \left[L, L; t, \tau\right] \frac{\partial p_2(L,\tau)}{\partial \tau} d\tau \,,$$

$$\mathcal{A}_{12}[p_2](t) = c_2 \int_0^{t-L_2/c_2} e^{-D_2(t-\tau)} I_0[L, L_1; t, \tau] \frac{\partial p_2(L_1,\tau)}{\partial \tau} d\tau \,,$$

$$\mathcal{A}_{13}[\dot{u}_{1|\Gamma}](t) = \frac{L_2}{c_2} \int_0^{t-L_2/c_2} I_0[L, L_1; t, \tau] \frac{\partial}{\partial \tau} \Big[\frac{\partial u_1(L_1,\tau)}{\partial \tau} \frac{e^{-D_2(t-\tau)}}{t-\tau} \Big] d\tau \,,$$

$$\mathcal{A}_{21}[p_2^L](t) = c_2 \int_0^{t-L_2/c_2} e^{-D_2(t-\tau)} I_0[L, L_1; t, \tau] \frac{\partial p_2(L,t)(\tau)}{\partial \tau} \, d\tau \,,$$

$$\mathcal{A}_{22}[p_2](t) = c_2 \int_0^t e^{-D_2(t-\tau)} I_0[L, L; t, \tau] \frac{\partial p_2(L_1,t)(\tau)}{\partial \tau} \, d\tau \,,$$

$$\mathcal{A}_{23}[\dot{u}_{1|\Gamma}](t) = -\dot{u}_1(L_1, t) \,,$$

$$\mathcal{A}_{31}[p_2^L](t) = \frac{L_2}{c_2} \int_0^{t-L_2/c_2} I_0[L, L_1; t, \tau] \frac{\partial}{\partial \tau} \Big[\frac{\partial p_2(L,\tau)}{\partial \tau} \frac{e^{-D_2(t-\tau)}}{t-\tau} \Big] \, d\tau \,,$$

$$\mathcal{A}_{32}[p_2](t) = -p_2(L_1, t) \,,$$

$$\mathcal{A}_{33}[u_{1|\Gamma}](t) = -\frac{D_2}{c_2} u_1(L_1, t) - \frac{1}{c_2} \dot{u}_1(L_1, t) - \int_0^t \frac{\partial I_0[L_1, L_1; t, \tau]}{\partial \tau} \frac{e^{-D_2(t-\tau)}}{c_2(t-\tau)} u_1(L_1, \tau) \, d\tau$$

and the bilinear form $\mathcal{A}(\cdot,\cdot)$ is defined exactly as in (21); further

$$\begin{aligned}
\mathcal{F}_1(q_2^L) &= \int_0^T \dot{\overline{u}}(t) q_2^L(t) dt\,, \\
\mathcal{F}_2(q_2) &= \int_0^T \int_0^{t-\frac{L_2}{c_2}} \frac{L_2}{c_2} I_0\left[L_1, L; t, \tau\right] \frac{\partial}{\partial \tau}\left(\dot{\overline{u}}(\tau)\frac{e^{-D_2(t-\tau)}}{\tau - t}\right) q_2(t) d\tau dt\,, \\
\mathcal{F}_3(\dot{v}_1) &= -\int_0^T \int_0^{t-\frac{L_2}{c_1}} I_0\left[L_1, L; t, \tau\right] \left\{ \frac{L_2^2}{c_2^3}\frac{\partial}{\partial \tau}\left(\overline{u}(t)\frac{e^{-D_2(t-\tau)}}{(\tau-t)^3}\right)\right. \\
&+ \left. \frac{L_2^2}{c_2^3}\frac{\partial^2}{\partial \tau^2}\left(\overline{u}(t)\frac{e^{-D_2(t-\tau)}}{(\tau-t)^2}\right) + \frac{1}{c_2}\frac{\partial}{\partial \tau}\left(\overline{u}(t)\frac{e^{-D_2(t-\tau)}}{\tau-t}\right)\right\} \dot{v}_1(L_1, t) d\tau dt \\
&- 2\int_0^T \overline{p}(t)\dot{v}_1(0,t) dt + 2\int_{\Omega_1}\int_0^T f_1(x,t)\dot{v}_1(x,t) dt dx.
\end{aligned}$$

In addition to $p_2(L_1, t)$ and $u_1(x, t)$ approximated as in (28), the further unknown $p_2^L(t)$ in the bounded bi-domain will be approximated as

$$p_2^L(t) \approx \widetilde{p}_2(L, t)(t) = \sum_{k=0}^{N_{\Delta t}-1} \gamma_k \overline{\psi}_k(t)\,. \tag{53}$$

The discretization of the energetic weak formulation (52) produces the linear system $\mathrm{M}\,\mathrm{x} = \mathrm{y}$ where matrix M has the same block lower triangular Toeplitz structure shown in (29) and the unknowns are organized as follows:

$$\mathrm{x}^{(\ell)} = \left(\gamma_\ell,\, \alpha_\ell,\, \beta_{\ell 0},\, \beta_{\ell 1}, \ldots, \beta_{\ell N_{\Delta x}}\right)^\top, \qquad \ell = 0, \ldots, N_{\Delta t} - 1\,.$$

Note that each matrix block is symmetric, highly sparse and it has the following structure:

$$\mathrm{M}^{(\ell)} = \begin{pmatrix} \mathrm{M}_{BEM}^{(\ell)} & \mathrm{M}_{BEM,\Gamma}^{(\ell)} & 0 \\ \mathrm{M}_{\Gamma,BEM}^{(\ell)} & \mathrm{M}_{\Gamma}^{(\ell)} & \mathrm{M}_{\Gamma,FEM}^{(\ell)} \\ 0 & \mathrm{M}_{FEM,\Gamma}^{(\ell)} & \mathrm{M}_{FEM}^{(\ell)} \end{pmatrix}$$

where diagonal sub-blocks have dimensions 1, 2, $N_{\Delta x}$, respectively, and whose elements have been evaluated numerically by means of adaptive Simpson rule.

6. NUMERICAL RESULTS

Example I: homogeneous parameters in BEM and FEM subdomains, smooth data.
Let us consider the unbounded interval configuration described in Sec. 2 with $L_1 = 1$. The parameters in the two subdomains have been considered equal: $c_1 = c_2 = \overline{c}$, $D_1 = D_2 = \overline{D}$ and $P_1 = P_2 = \overline{P}$.
At the end-point $x = 0$ of the bounded portion, the smooth Neumann datum $\bar{p}(t) = 3\,t^2$ is given and the source term in Ω_1 has been chosen as

$$f_1(x,t) = 6\,t^2(1-x) - \frac{(1-x)^3}{\overline{c}^2}(2 + 4\overline{D}t + \overline{P}t^2)\,.$$

In this case, problem (1)-(5) has solution given by

$$u(x,t) = \begin{cases} u_1(x,t) = t^2(1-x)^3, & 0 \le x \le 1 \\ u_2(x,t) = 0, & x > 1 \end{cases} . \tag{54}$$

	$\bar{c}=1;\bar{P}=1;\bar{D}=0$		$\bar{c}=1;\bar{P}=0;\bar{D}=1$		$\bar{c}=1;\bar{P}=1;\bar{D}=1$	
s	E_s	$\log_2[\frac{E_{s-1}}{E_s}]$	E_s	$\log_2[\frac{E_{s-1}}{E_s}]$	E_s	$\log_2[\frac{E_{s-1}}{E_s}]$
0	$3.628 \cdot 10^{-2}$		$2.205 \cdot 10^{-2}$		$2.081 \cdot 10^{-2}$	
1	$2.039 \cdot 10^{-2}$	0.831	$1.239 \cdot 10^{-2}$	0.823	$1.180 \cdot 10^{-2}$	0.818
2	$1.087 \cdot 10^{-3}$	0.908	$6.593 \cdot 10^{-3}$	0.910	$6.306 \cdot 10^{-3}$	0.904
3	$5.628 \cdot 10^{-3}$	0.950	$3.408 \cdot 10^{-3}$	0.952	$3.265 \cdot 10^{-3}$	0.950
4	$2.867 \cdot 10^{-3}$	0.973	$1.734 \cdot 10^{-3}$	0.975	$1.663 \cdot 10^{-3}$	0.973
5	$1.448 \cdot 10^{-3}$	0.986	$8.748 \cdot 10^{-4}$	0.987	$8.395 \cdot 10^{-4}$	0.986
6	$7.278 \cdot 10^{-4}$	0.993	$4.395 \cdot 10^{-4}$	0.993	$4.218 \cdot 10^{-4}$	0.993

Table 1: Errors E_s, defined as in (30), and experimental convergence order for $\Delta x = \Delta t = 0.1 \times 2^{-s}$.

For final time of investigation $T = 1$, in Table 1, we show the error E_s defined in (30) and the experimental convergence order, obtained by energetic BEM-FEM coupling approach, starting with a fixed mesh in time and in space and then halving each time Δt and Δx: results are in accordance with the recalled estimate.
In Table 2, we can observe that the approximate solution converges, in maximum-norm over Ω_1, toward the exact solution independently refining the discretization parameters, even when assigning big values to velocity or

damping coefficients; in particular, when considering high velocities it is necessary to tighten time grid in order to adapt the discrete velocity $\Delta x/\Delta t$ to the exact one, while, when one of the damping coefficient increases, it is necessary to tighten space mesh in order to capture the damping process along the domain.

$\overline{c} = 100,\ \overline{D} = 0,\ \overline{P} = 0$

Δt \ Δx	0.1	0.05	0.025	0.0125
0.1	$2.985 \cdot 10^{-3}$	$2.983 \cdot 10^{-3}$	$2.983 \cdot 10^{-3}$	$2.983 \cdot 10^{-3}$
0.05	$6.558 \cdot 10^{-4}$	$6.525 \cdot 10^{-4}$	$6.525 \cdot 10^{-4}$	$6.523 \cdot 10^{-4}$
0.025	$2.985 \cdot 10^{-4}$	$1.153 \cdot 10^{-4}$	$1.151 \cdot 10^{-4}$	$1.152 \cdot 10^{-5}$
0.0125	$2.441 \cdot 10^{-4}$	$5.765 \cdot 10^{-5}$	$3.116 \cdot 10^{-5}$	$3.130 \cdot 10^{-5}$

$\overline{c} = 1,\ \overline{D} = 100,\ \overline{P} = 0$

Δt \ Δx	0.1	0.05	0.025	0.0125
0.1	$1.132 \cdot 10^{-1}$	$2.863 \cdot 10^{-2}$	$7.441 \cdot 10^{-3}$	$2.140 \cdot 10^{-3}$
0.05	$1.128 \cdot 10^{-1}$	$2.828 \cdot 10^{-2}$	$7.087 \cdot 10^{-3}$	$1.786 \cdot 10^{-3}$
0.025	$--$	$2.823 \cdot 10^{-2}$	$7.036 \cdot 10^{-3}$	$1.735 \cdot 10^{-3}$
0.0125	$--$	$--$	$7.042 \cdot 10^{-3}$	$1.741 \cdot 10^{-3}$

$\overline{c} = 1,\ \overline{D} = 0,\ \overline{P} = 100$

Δt \ Δx	0.1	0.05	0.025	0.0125
0.1	$1.139 \cdot 10^{-1}$	$2.977 \cdot 10^{-2}$	$8.695 \cdot 10^{-3}$	$4.319 \cdot 10^{-3}$
0.05	$1.126 \cdot 10^{-1}$	$2.852 \cdot 10^{-2}$	$7.449 \cdot 10^{-3}$	$2.789 \cdot 10^{-3}$
0.025	$1.123 \cdot 10^{-1}$	$2.821 \cdot 10^{-2}$	$7.128 \cdot 10^{-3}$	$1.855 \cdot 10^{-3}$
0.0125	$1.122 \cdot 10^{-1}$	$2.811 \cdot 10^{-2}$	$7.027 \cdot 10^{-3}$	$1.758 \cdot 10^{-3}$

Table 2: Maximum norm error over Ω_1 w.r.t. the exact solution $u_1(x,t) = t^2(1-x)^3$.

Example II: homogeneous parameters in BEM and FEM subdomains, non-smooth data.
Let us consider again the unbounded interval configuration in Sec. 2 with $L_1 = 1$. The parameters in the two subdomains have been still considered equal: $c_1 = c_2 = \overline{c}$, $D_1 = D_2 = \overline{D}$ and $P_1 = P_2 = \overline{P}$. Considering trivial source force $f_1(x,t) = 0$ and applying the non-smooth Neumann boundary

condition $\overline{p}(t) = H[t-0.5] - H[t-1]$ the explicit solution becomes

$$\forall x \in \Omega = \Omega_1 \cup \Omega_2, \quad u(x,t) = 2\int_0^t G(x,0;t-0.5,\tau)d\tau - 2\int_0^t G(x,0;t-1,\tau)d\tau.$$

Varying the material parameters, we can observe their influence on the solution and in particular the diffusive nature of damping which seeks to distribute the energy throughout the structure. The following figures represent the numerical solution at $x = 0$ and at the interface $x = L_1$, evaluated with $\Delta x = \Delta t = 0.05$ on time interval $[0, 5]$.

Let us start with the simple case $\overline{D} = \overline{P} = 0$. In Fig. 1 we observe, as expected, that, augmenting $\overline{c}$ from the value 1 to the value 10, the wave moves more rapidly, reducing the time gap between $u(0,t)$ and $u(L_1,t)$ (note that the wave hits the interface at the time instant $L_1/\overline{c}$) and increasing its amplitude proportionally to $\overline{c}$.

Then, fixing $\overline{c} = 1$, $\overline{P} = 0$ and augmenting the viscous damping coefficient $\overline{D}$ from the value 1 to the value 10, the dissipation implying a faster vanishing of the wave is increased, as highlighted in Fig. 2. This phenomenon was clearly expected since the fundamental solution $G(x, y; t, \tau)$ in (7) presents a time decay depending on D_2.

In Fig. 3 we see the effect of increasing $\overline{P}$, having fixed $\overline{c} = 1$, $\overline{D} = 0$: the material damping behaves like a restoring force opposing to the displacement and giving rise to an oscillatory behavior. At last, in Fig. 4 we show the combined effect of $\overline{P}$ and $\overline{D}$.

Note that oscillations in the solution appear if the magnitude of $\overline{P}$ is bigger than that of $\overline{D}^2$: this can be justified by the presence of alternating sign terms in the definition of the Bessel function $I_0[x, y; t, \tau]$; the overall decay behavior is that of the fundamental solution G.

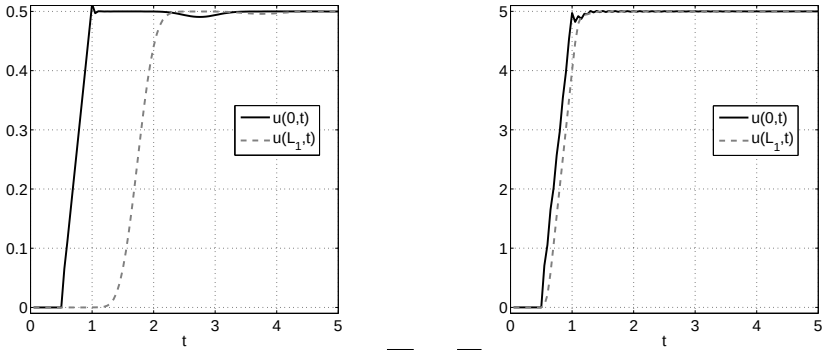

Figure 1: Numerical solution with $\overline{D} = \overline{P} = 0$, $\overline{c} = 1$ on the left and $\overline{c} = 10$ on the right.

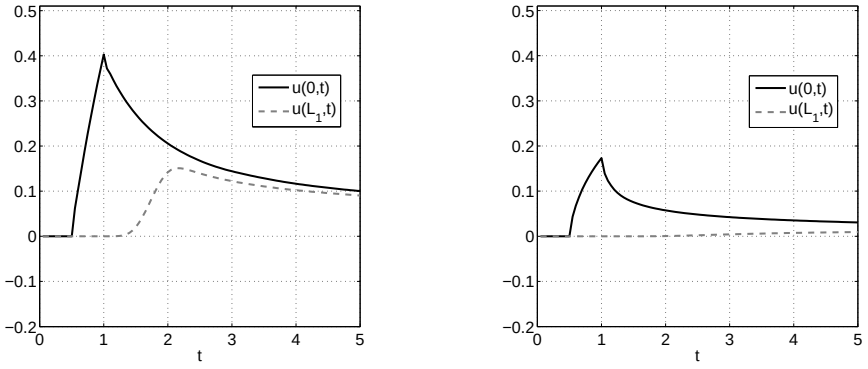

Figure 2: Numerical solution with $\overline{c} = 1$, $\overline{P} = 0$, $\overline{D} = 1$ on the left and $\overline{D} = 10$ on the right.

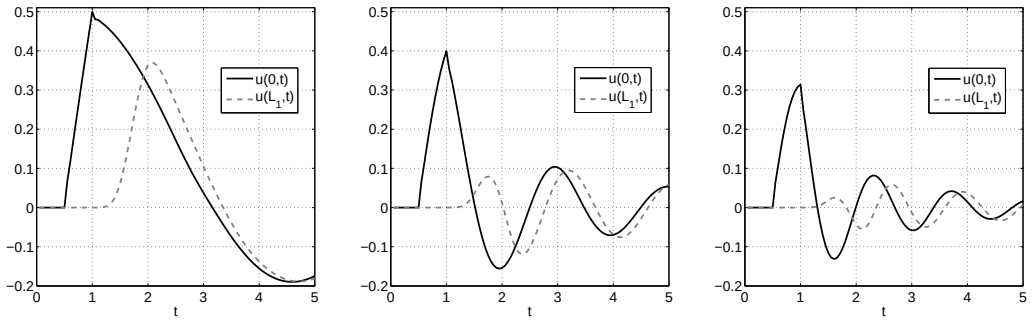

Figure 3: Numerical solution with $\overline{c} = 1$, $\overline{D} = 0$, $\overline{P} = 1, 10, 20$ from left to right.

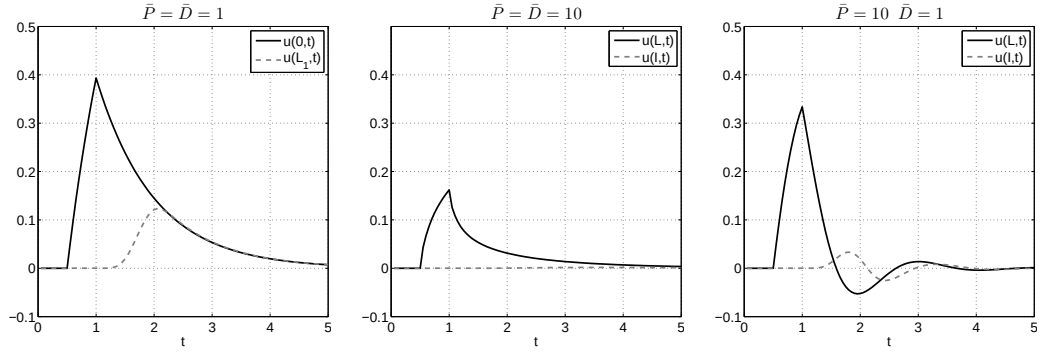

Figure 4: Numerical solution with $\overline{c} = 1$ and from left to right $\overline{D} = \overline{P} = 1, 10$ and $\overline{D} = 1, \overline{P} = 10$.

We conclude underlying that the approximate solutions of all the above presented simulation are in very good agreement with the corresponding analytical ones.

Example III: non-homogeneous parameters in BEM and FEM subdomains, non-smooth data.
Let us consider for the last time the unbounded interval configuration in Sec. 2 with $L_1 = 1$. In this example $f_1(x,t)$ is still trivial and the discretization parameters are fixed as $\Delta x = \Delta t = 0.05$. With rectangular impulse $\bar{p}(t) = c_1^{-2}(H[t] - H[t - 0.25])$ as Neumann boundary condition, we investigate the solution in the time interval $[0, 10]$ assuming physical parameters not necessarily equal in the two subdomains and analyzing the resulting approximate solutions behavior.
In Fig. 5 on the left the damping parameters are set equal to 0 therefore the equation (1) reduces to the 1D wave equation without damping; we observe that, when we have different velocities in Ω_2 (BEM) and Ω_1 (FEM) subdomains, i.e. $c_2 \neq c_1$, the graph of $u(0,t)$ initially overlaps the solution obtained considering the same velocity c_1 in both subdomains, and definitely it decays over the solution obtained considering the same velocity c_2 in both subdomains. The same behavior can be observed if we vary damping parameters, for example assuming non trivial material damping, as shown in Fig. 5 on the right.
Having fixed $c_1 = c_2 = 1$ and $D_1 = D_2 = 0$ in Ω_1 and Ω_2, in Fig. 6 on the left, we observe that the graphs of $u(0,t)$ with different material damping initially overlaps the solutions obtained with equal parameters in both subdomains. When $P_1 = 1$ and $P_2 = 0$, i.e. we are solving the damped wave equation in the FEM subdomain and the wave equation in the BEM subdomain, the wave traveling from the loaded endpoint finds a sort of "transparent" condition at the interface point and the solution $u(0,t)$ has the fastest decay to zero among all approximate solutions, while when $P_1 = 0$ and $P_2 = 1$, i.e. we are solving the wave equation in the FEM subdomain and the damped wave equation in the BEM subdomain, the wave traveling from the loaded endpoint finds a sort of "wall" at the interface point and the solution $u(0,t)$ presents more oscillations. This behavior is stressed in Figure 6 on the right, where the time history $u(0,t)$ at the loaded end-point is shown for $P_1 = 0$ and growing P_2: the solution tends to that of the wave equation with unitary velocity, defined on the spatial bounded interval $\Omega = (0, L_1)$ with $L_1 = 1$, equipped with mixed boundary condition: $p(0,t) = H(t) - H(t - 0.25)$, $u(L_1,t) = 0$.

Also in Fig. 7 on the left, we observe that the graphs of $u(0,t)$ for different viscous damping parameters in Ω_1 , Ω_2 initially overlap the corresponding solution obtained considering the same viscous damping $D_1 = D_2$ in both subdomains, and then the different damping coefficient D_2 damps down the wave or, viceversa, when trivial, it keeps the solution constant.

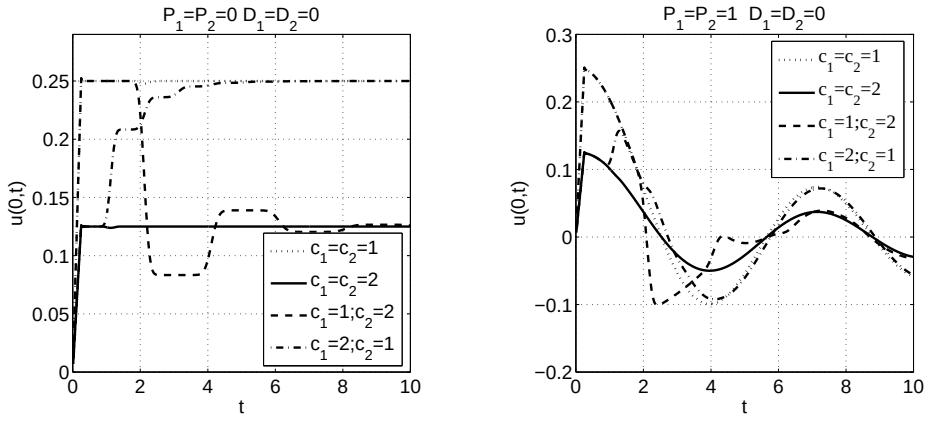

Figure 5: Graphs of $u(0,t)$ changing velocities in the two subdomains: on the left with damping parameters equal to 0, on the right with non trivial material damping.

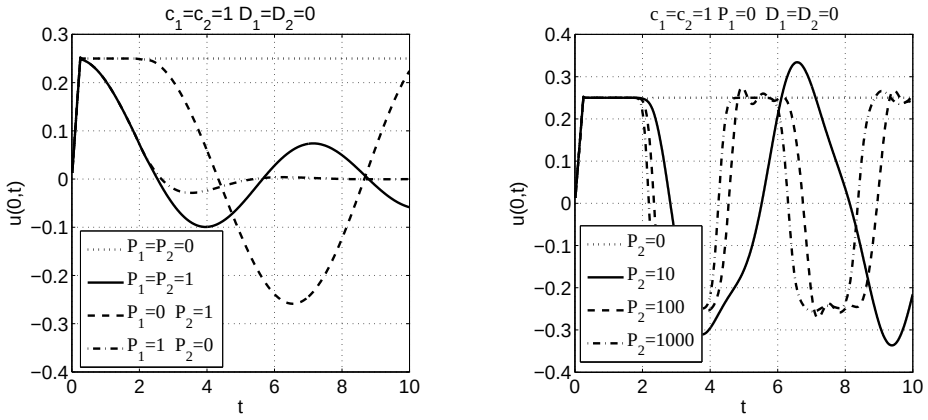

Figure 6: Graphs of $u(0,t)$ changing material damping.

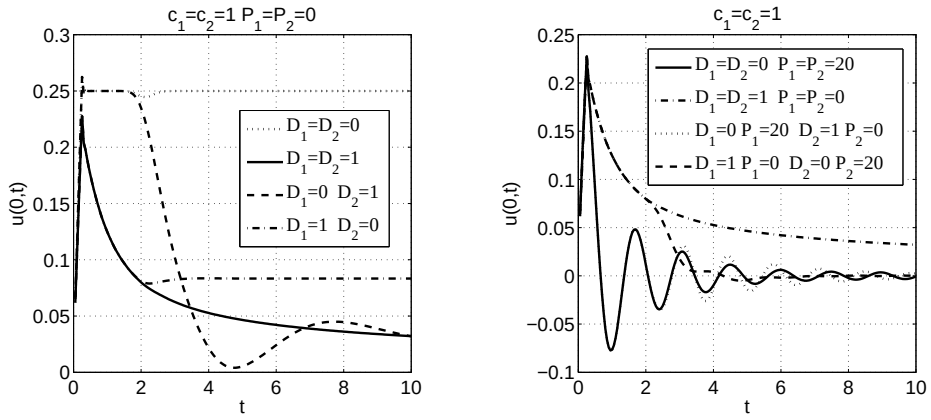

Figure 7: On the left: graphs of $u(0,t)$ changing viscous damping. On the right: graphs of $u(0,t)$ changing both material and viscous damping.

In Fig. 7 on the right, there is clear evidence that, changing both material and viscous damping coefficients, the stability of the numerical solution is kept along the entire time interval of analysis.

Example IV: application of energetic BEM alone.
Here, we consider the bounded domain of Sec. 5, where we fix $\Omega_1 = \emptyset$ and $\Omega \equiv \Omega_2 = [0, L]$, in order to compare results coming from the presented energetic approach to those found in literature for the damped wave equation treated by BEM. In fact, we test the energetic BEM applied to the one-dimensional damped wave propagation problem in a bounded mono-domain considering the following example, taken from [16], which solves the same differential problem using a fully boundary element formulation too. In that paper, as here, the Authors consider the free-space Green's function G given in (7) incorporating both viscous and material damping, D_2 and P_2 respectively, but their discretization method is based on a collocation BEM.
In particular, in [16], problem (1)-(4) is related to a rod fixed in the right end-point $x = L = 1$ (i.e. the Dirichlet condition (48) is $\bar{u}(t) = 0$), while on the left end-point $x = 0$ a traction $\bar{p}(t)$ is applied. For this kind of configuration the analytical solution, useful for comparison with numerical results, is known: $\forall x \in \Omega$, $\forall t \in [0, T]$

$$u(x,t) = \sum_{n=1}^{+\infty} (-1)^{n-1} \int_0^{+\infty} 2\big[G\big(x, -2(n-1)L; t, \tau\big) - G\big(x, 2nL; t, \tau\big)\big]\bar{p}(\tau)d\tau\,. \quad (55)$$

In order to investigate the effect of material damping in structures, a single

pulse traction $\bar{p}(t) = H[t] - H[t - 1/4]$ is applied.

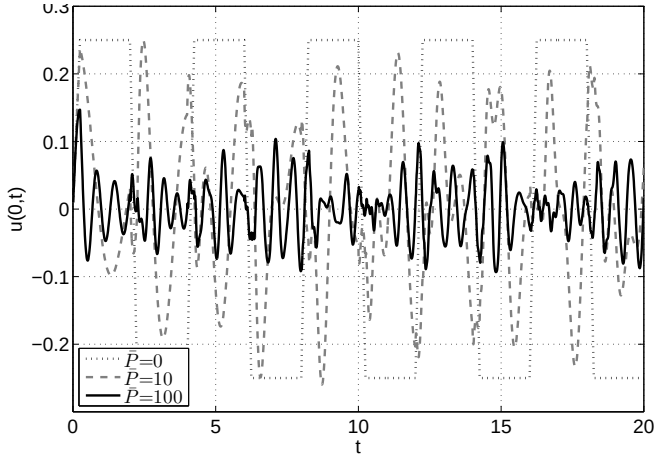

Figure 8: $u(0,t)$ for $\bar{p}(t) = H[t] - H[t-1/4]$, $c_2 = 1$, $D_2 = 0$, varying $P_2 = \bar{P}$.

Δt	$P_2 = \bar{P} = 10$	$P_2 = \bar{P} = 100$
0.2	$3.07 \cdot 10^{-1}$	$1.68 \cdot 10^{-1}$
0.1	$1.14 \cdot 10^{-1}$	$1.11 \cdot 10^{-1}$
0.05	$3.11 \cdot 10^{-2}$	$5.53 \cdot 10^{-2}$
0.025	$8.47 \cdot 10^{-3}$	$2.81 \cdot 10^{-2}$
0.01	$3.27 \cdot 10^{-3}$	$1.81 \cdot 10^{-2}$

Table 3: Table of errors in L^2-norm in time, w.r.t. the analytical solution (55) at $x = 0$.

In Fig. 8, $u(0,t)$ has been computed starting from energetic boundary element formulation applied to the BIEs coming from (6) and (9) evaluated at $x = L$ and at $x = 0$ respectively, using $\Delta t = 0.01$, assuming $c_2 = 1$ and $D_2 = 0$ and varying $P_2 = \bar{P}$; in any case, the approximation overlaps the analytical solution. Furthermore, Table 3 shows the convergence towards the analytical solution (55), using $L^2([0,1])$-norm in time and refining the discretization parameter Δt.
In Fig. 9, we emphasize convergence, for the case $P_2 = \bar{P} = 10$ in the time interval $[0, 4]$.

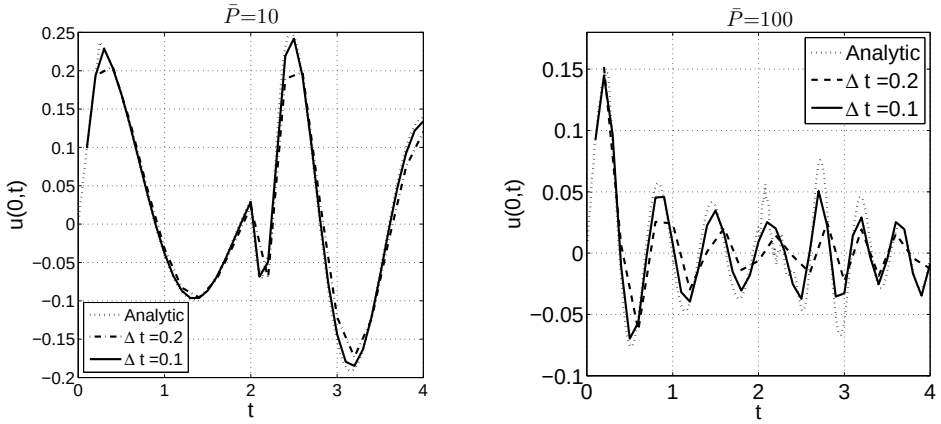

Figure 9: Focus of solution $u(0,t)$ in the interval $[0,4]$, as in [16].

In order to investigate the diffusive nature of viscous damping in structures, the repetitive pulse traction represented in Fig. 10 is now applied.

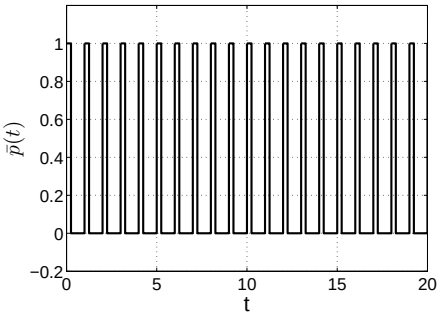

$$\bar{p}(t) = \sum_{n=0}^{\infty} H[t-n] - H[t-n-1/4]$$

Figure 10: Repetitive pulse traction.

The approximate solution $u(0,t)$, depicted in Fig. 11 reproduces the analytical one that can be obtained substituting the above Neumann condition in (55).

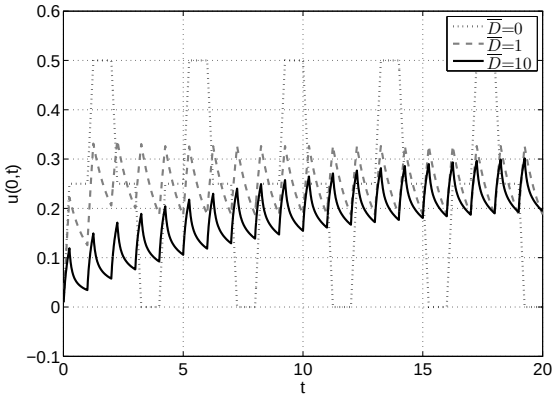

Figure 11: $u(0,t)$ for $\bar{p}(t)$ as given in Fig.10, $c_2 = 1$, $P_2 = 0$, varying $D_2 = \bar{D}$.

In Fig. 12 and Table 4, we emphasize convergence.

Δt	$D_2 = \bar{D} = 1$	$D_2 = \bar{D} = 10$
0.2	$3.14 \cdot 10^{-2}$	$2.35 \cdot 10^{-2}$
0.1	$1.59 \cdot 10^{-2}$	$1.59 \cdot 10^{-2}$
0.05	$1.77 \cdot 10^{-3}$	$2.97 \cdot 10^{-3}$
0.025	$1.73 \cdot 10^{-3}$	$2.23 \cdot 10^{-3}$
0.01	$1.73 \cdot 10^{-3}$	$2.20 \cdot 10^{-3}$

Table 4: Table of errors in L^2-norm in time, w.r.t. the analytical solution (55) at $x = 0$.

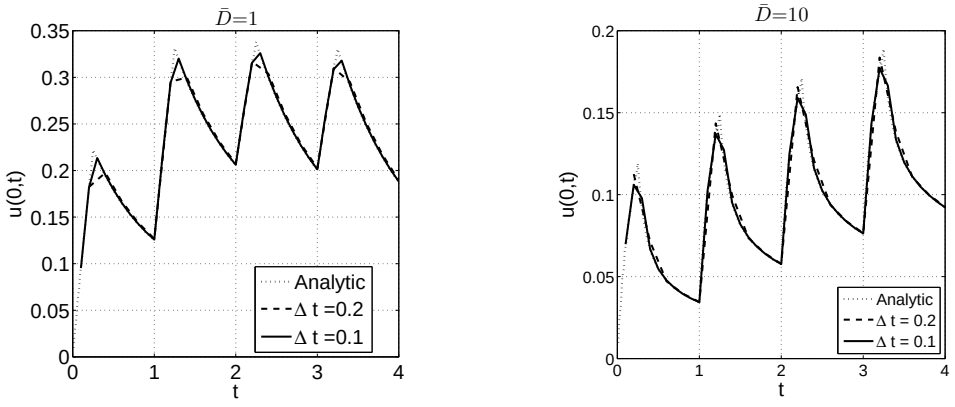

Figure 12: Focus of solution $u(0,t)$ in the interval $[0,4]$, as in [16], emphasizing convergence.

We note that in all cases no instabilities appear and the approximate solutions are in agreement with the exact ones also considering time intervals much longer (quintuple) than those investigated in [16].

Example V: application of energetic BEM-FEM.
The following example still takes into consideration the bounded domain of Sec. 5, Ω, split in two sub-domains of equal length with $L_1 = L_2 = 0.5$, $\bar{u}(t) = 0$ assigned at $x = L = 1$ and the traction $\bar{p}(t) = H[t]$ applied at $x = 0$.
We fix the discretization parameters $\Delta x = 0.05$ and $\Delta t = 0.01$ and, assuming $c_1 = c_2 = \bar{c} = 1$, $D_1 = D_2 = \bar{D} = 0$ and $P_1 = 0$, we increase the material damping P_2 in the BEM sub-domain Ω_2, observing the evolution of the behavior of $u(0,t)$ and $u(L_1,t)$.
If $P_2 = 0$, as in FEM sub-domain Ω_1, the approximated solution behaves like the analytical solution of the wave equation without damping, both in $x = 0$ and $x = L_1$; in the limit $P_2 \to +\infty$, the wave tends to be completely reflected by the BEM sub-domain: in fact the bold lines in Fig. 13 represent an approximation of the analytical solution of the wave equation without damping for a rod of length $L_1 = 0.5$ with boundary conditions $\bar{u}(t) = 0$ at $x = L_1$ and $\bar{p}(t) = H[t]$ at $x = 0$.

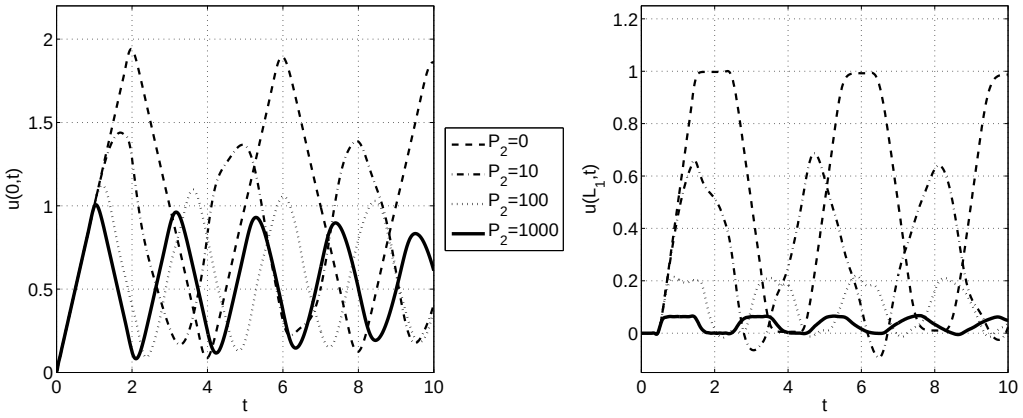

Figure 13: $u(0,t)$ on the left and $u(L_1,t)$ on the right for different values of P_2.

7. Conclusions

The advantages of BEM, when compared to domain methods, are well known, particularly in presence of unbounded domains. Further, for volume forces in small portions of the problem domain, the coupling of FEM with BEM reveals very advantageous.
In this paper, we have shown the efficiency of the energetic formulation in the case of 1D damped wave propagation problems, with theoretical results and several numerical examples, both for BEM and BEM-FEM techniques.
Due to the optimal performances obtained in all the simulations, we are now actually extending the energetic approach to the numerical solution of damped wave propagation problems in 2D space dimension.

References

[1] H. Antes, G. Beer, W. Moser, Soil-structure interaction and wave propagation problems in 2D by a duhamel integral based approach and the convolution quadrature method, Comput. Mech 36 (6) (2005) 431–443.

[2] A. Bachelot, L. Bounhoure, A. Pijols, Couplage éléments finis–potentiels retardés pour la diffraction électromagnétique par un obstacle hétérogène, Numer. Math. 89 (2001) 257–306.

[3] D. Beskos, G. Maier, Boundary element advances in solid mechanics, Springer, 2003.

[4] T. Cruse, F. Rizzo, A direct formulation and numerical solution of the general transient elastodynamic problem-I, J. Math. Anal. Appl. 22 (1968) 244–259.

[5] A. Frangi, Elastodynamics by BEM: a new direct formulation, International Journal for Numerical Methods in Engineering 45 (1999) 721–740.

[6] M. Schanz, Application of 3D boundary element formulation to wave propagation in poroelastic solids, Eng. Anal. Boundary Elem. 25 (2001) 363–376.

[7] A. Bamberger, T. Ha Duong, Formulation variationelle espace-temps pour le calcul par potential retardé de la diffraction d'une onde acoustique (I), Mathematical Methods in the Applied Sciences 8 (1986) 405–435.

[8] A. Bamberger, T. Ha Duong, Formulation variationelle pour le calcul de la diffraction d'une onde acoustique par une surface rigide, Mathematical Methods in the Applied Sciences 8 (1986) 598–608.

[9] C. Lubich, Convolution quadrature and discretized operational calculus I, Numerische Mathematik 52 (1988) 129–145.

[10] C. Lubich, Convolution quadrature and discretized operational calculus II, Numerische Mathematik 52 (1988) 413–425.

[11] A. Aimi, M. Diligenti, A new space-time energetic formulation for wave propagation analysis in layered media by BEMs, Int. J. Numer. Meth. Engng. 75 (2008) 1102–1132.

[12] A. Aimi, S. Gazzola, C. Guardasoni, Energetic boundary element method analysis of wave propagation in 2D multilayered media, Mathematical Methods in Applied Sciences 35 (2012) 1140–1160.

[13] A. Frangi, G. Novati, On the numerical stability of time-domain elastodynamic analyses by BEM, Computer Methods in Applied Mechanics and Engineering 173 (1999) 403–417.

[14] T. Ha Duong, On retarded potential boundary integral equations and their discretization, in: P. D. et al. (Ed.), Topics in computational wave propagation. Direct and inverse problems, Springer-Verlag, 2003, pp. 301–336.

[15] G. Maier, M. Diligenti, A. Carini, A variational approach to boundary element elasto-dynamic analysis and extension to multidomain problems, Comput. Methods Appl. Mech. Engrg. 92 (1991) 193–213.

[16] A. Vick, R. West, Analysis of Damped Wave Using the Boundary Element Method, Transaction on Modelling and Simulation 15 (1997) 265–278.

[17] A. Aimi, L. Desiderio, M. Diligenti, C. Guardasoni, A numerical study of energetic BEM-FEM applied to wave propagation in 2D multidomains, Publications de l'Institut Mathmatique - Beograd 96 (110) (2014) 5–22.

[18] A. Aimi, M. Diligenti, A. Frangi, C. Guardasoni, Energetic BEM-FEM coupling for wave propagation in 3D multidomains, Int. J. Num. Meth. Engng. 97 (2014) 377–394.

[19] A. Aimi, M. Diligenti, C. Guardasoni, S. Panizzi, Energetic BEM-FEM coupling for wave propagation in layered media, Communications in Applied and Industrial Mathematics (2013) DOI: 10.1685/journal.caim.438.

[20] A. Aimi, S. Panizzi, BEM-FEM coupling for the 1D Klein-Gordon equation, Numer. Methods Partial Differential Equations 30 (6) (2014) 2042–2082.

[21] M. Costabel, Time-dependent problems with the boundary integral equation method, in: E. S. et al. (Ed.), Encyclopedia of Computational Mechanics, John Wiley and Sons, 2004, pp. 1–28.

[22] A. Quarteroni, A. Valli, Numerical Approximation of Partial Differential Equations, Springer-Verlag, 1994.